Supporting Information

π-Bridge-Independent 2-(Benzo[*c*][1,2,5]thiadiazol-4-ylmethylene)malononitrile-Substituted Nonfullerene Acceptors for Efficient BHJ Solar Cells

*Kai Wang,[†,§] Yuliar Firdaus,[†,§] Maxime Babics,[†] Federico Cruciani,[†] Qasim Saleem,[†] Abdulrahman El Labban,[†] Maha A. Alamoudi,[†] Tomasz Marszalek,[‡] Wojciech Pisula,[‡,#] Frederic Laquai,[†] and Pierre M. Beaujuge[†,]**

[†]***Physical Sciences and Engineering Division, Solar & Photovoltaic Engineering Research Center (SPERC), King Abdullah University of Science and Technology (KAUST), Thuwal 23955-6900, Saudi Arabia;*** [‡]***Max Planck Institute for Polymer Research, Ackermannweg 10, D-55128 Mainz, Germany;*** [#]***Department of Molecular Physics, Faculty of Chemistry, Lodz University of Technology, Zeromskiego 116, 90-924 Lodz, Poland***

*To whom correspondence should be addressed. Email: pierre.beaujuge@kaust.edu.sa

Content:

1. General Experimental Details

Methods and Materials: All reagents from commercial sources were used without further purification. Solvents were dried and purified using standard techniques. Reactions were carried out under nitrogen atmosphere when appropriate. Microwave-assisted reactions were performed in a Biotage Initiator (Initiator+). Flash chromatography was performed with analytical-grade solvents using Silicycle Silica Flash P60 (particle size 40-63 μm, 60 Å, 230 – 400 mesh) silica gel. Flexible TLC plates PE SilG/UV 250μm from Whatman were used for TLC. Recycling SEC in THF or ethanol-blended chloroform was carried out through a set of two JAIGEL-4H-40 preparative SEC columns mounted on a LC-9130NEXT (JAI) system equipped with coupled UV-254NEXT and RI-700NEXT detectors. All compounds were characterized by NMR spectroscopy on Bruker Avance III Ultrashield Plus instruments with 400 and 700 MHz proton frequency at the given temperatures. The spectra were referenced on the internal standard TMS. High-resolution mass spectrometry (HRMS) data was recorded using a Thermo Scientific - LTQ Velos Orbitrap MS. UV-Vis spectra in solution were recorded on a Varian Cary 100 instrument in single beam mode in 1 cm quartz cuvettes. Spectroscopy-grade $CHCl_3$ was filtered through basic alumina prior to use in order to suppress solvent acidity and avoid undesired protonation reactions that may influence the spectral absorption of the small-molecule analogues examined in this study.

2. Synthetic Procedures

Overview Scheme

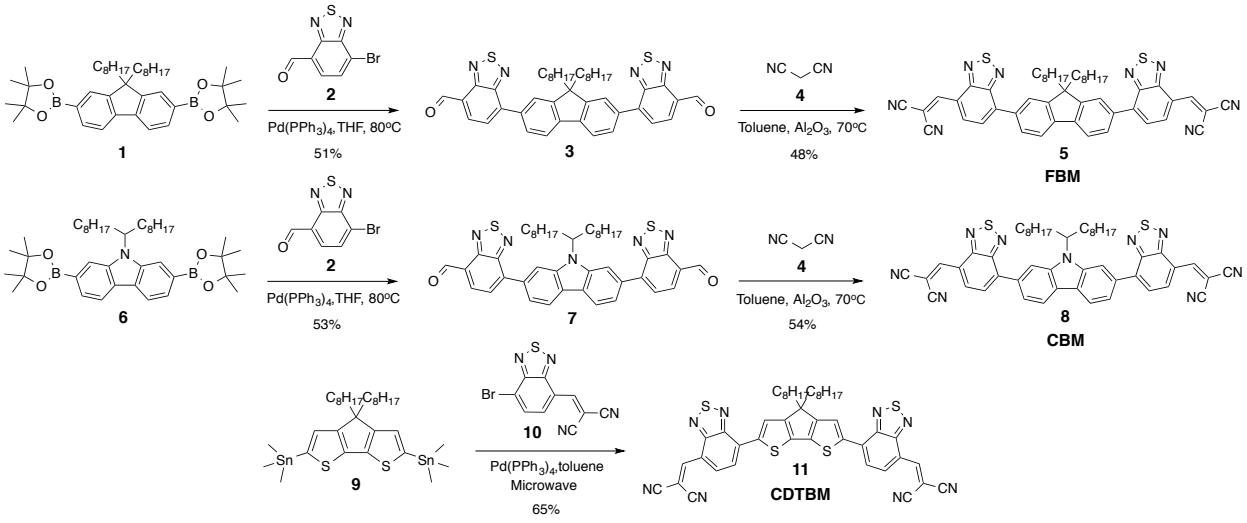

Note: 4-bromo-2,1,3-benzothiadiazole-4-carboxaldehyde **(2)**, 4-Bromo-7-dicyanovinyl-2,1,3-benzothiadiazole **(10)**, 7,7'-(9,9-dioctyl-9*H*-fluorene-2,7-diyl)dibenzo[*c*][1,2,5]thiadiazole-4-carbaldehyde **(3)** and 4,4-dioctyl-2,6-bis(trimethylstannanyl)-4*H*-cyclo-penta[2,1-*b*:3,4-*b*']dithiophene **(9)** were synthesized according to previously reported methods.[1-3]

7,7'-(9,9-dioctyl-9*H*-fluorene-2,7-diyl)dibenzo[*c*][1,2,5]thiadiazole-4-carbaldehyde (3): A solution of 2,2'-(9,9-dioctyl-9*H*-fluorene-2,7-diyl)bis(4,4,5,5-tetramethyl-1,3,2-dioxaborolane) **(1)** (0.31 g, 0.5 mmol) and 4-bromo-2,1,3-benzothiadiazole-4-carboxaldehyde **(2)** (278 mg, 1.15 mmol) in THF (30 ml) was degassed, and $Pd(PPh_3)_4$ (20 mg, 0.03 eq) was added to the reaction vessel. A solution of K_2CO_3 (1M, 1.5 ml) was then added to the reaction mixture, and the reaction was refluxed overnight. The reaction mixture was then cooled to room temperature, quenched with water and extracted with CH_2Cl_2. The organic phase was dried over sodium sulfate, the solvent was removed by rotary evaporation and the crude mixture was purified via column chromatography over SiO_2 with CH_2Cl_2 as the eluent, affording intermediate (**3**) as a red solid (164 mg, 46%). ^{1}H NMR (400 MHz, $CDCl_3$): δ 10.84 (s, 2H), 8.37 (d, J = 7.2 Hz, 2H), 8.12-7.98 (m, 8H), 2.17-2.14 (m, 4H), 1.19-1.09 (m, 20H), 0.88-0.85 (m, 4H), 0.79 (t, J = 7.0 Hz, 6H).

2,2'-(7,7'-(9,9-dioctyl-9*H*-fluorene-2,7-diyl)bis(benzo[*c*][1,2,5]thiadiazole-7,4-diyl))bis(methan-1-yl-1-ylidene)dimalononitrile (5, FBM): A mixture of 7,7'-(9,9-dioctyl-9*H*-fluorene-2,7-diyl)dibenzo[*c*][1,2,5]thiadiazole-4-carbaldehyde (**3**) (1100 mg, 1.54 mmol), malononitrile (**4**) (407 mg, 6.16 mmol), and basic aluminum oxide (2.2 g) in anhydrous toluene (60 mL) was heated to 70 °C and stirred for 2h. The reaction mixture was then cooled to room temperature, and the basic aluminum oxide residue was removed by filtration and thoroughly washed with toluene. The solvent of the filtrate was removed by rotary evaporation, and the crude product was purified via column chromatography over SiO_2 with CH_2Cl_2 as the eluent. The product fractions were pooled, concentrated and further purified by recycling SEC ($CHCl_3$), yielding **FBM** (**5**) as a red solid (610 mg, 48%). ^{1}H NMR (700 MHz, $CDCl_3$): δ 8.92 (s, 2H), 8.89 (d, J = 7.0 Hz, 2H), 8.16 (d, J = 7.0 Hz, 2H), 8.11 (s, 2H), 8.06 (d, J = 7.0 Hz, 2H), 8.01 (d, J = 7.0 Hz, 2H), 2.17-2.14 (m, 4H), 1.19-1.09 (m, 20H), 0.88-0.85 (m, 4H), 0.79 (t, J = 7.0 Hz, 6H), ^{13}C NMR (176 MHz, $CDCl_3$): δ 154.45, 153.05, 153.00, 152.29, 142.10, 140.80, 135.46, 130.71, 129.12, 127.35, 124.45, 122.48, 120.78, 113.76, 112.99, 83.35, 55.74, 40.16, 31.81, 30.02, 29.25, 24.97, 24.03, 22.62, 14.09. HRMS (+APCI, m/z): calcd. for $C_{49}H_{46}N_8S_2$ $[M+H]^+$: 811.33204; found 811.33552.

7,7'-(9-(heptadecan-9-yl)-9*H*-carbazole-2,7-diyl)dibenzo[*c*][1,2,5]thiadiazole-4-carbaldehyde (7): A solution of 9-(heptadecan-9-yl)-2,7-bis(4,4,5,5-tetramethyl-1,3,2-dioxaborolan-2-yl)-9*H*-carbazole **(6)** (2.52 g, 3.93 mmol) and 4-bromo-2,1,3-benzothiadiazole-4-carboxaldehyde **(2)** (2.2 g, 9.04 mmol) in THF (80 ml) was degassed, and $Pd(PPh_3)_4$ (136 mg, 0.03 eq) was added to the reaction vessel. A solution of K_2CO_3 (1M, 10 ml) was then added to the reaction mixture, and the reaction was refluxed overnight. The reaction mixture was then cooled to room temperature, quenched with water and extracted with CH_2Cl_2. The organic phase was dried over sodium sulfate, the solvent was removed by rotary evaporation and the crude mixture was purified via column chromatography over SiO_2 with CH_2Cl_2 as the eluent, affording intermediate (**7**) as a red solid (1.52g, 53%). ^{1}H NMR (700 MHz, $CDCl_3$): δ 10.85 (s, 2H), 8.47 (s, 1H), 8.40 (d, J = 7.0 Hz, 2H), 8.37 (d, J = 7.0 Hz, 1H), 8.34 (d, J = 7.0 Hz, 1H), 8.24 (s, 1H), 8.08 (d, J = 7.0 Hz, 2H), 7.88 (d, J = 7.0 Hz, 2H), 4.79 (m, 1H), 2.50-2.45 (m, 2H), 2.07-2.02 (m, 2H), 1.35-1.10 (m, 24H), 0.79 (t, J = 7.0 Hz, 6H). HRMS (+APCI, m/z): calcd. for $C_{49}H_{46}N_8S_2$ $[M+H]^+$: 730.32047; found 730.32485.

2,2'-(7,7'-(9-(heptadecan-9-yl)-9*H*-carbazole-2,7-diyl)bis(benzo[*c*][1,2,5]thiadiazole-7,4-diyl))bis(methan-1-yl-1-ylidene)dimalononitrile (8, CBM): A solution of 7,7'-(9-(heptadecan-9-yl)-9*H*-carbazole-2,7-diyl)dibenzo[*c*][1,2,5]thiadiazole-4-carbaldehyde **(7)** (0.27 g, 0.37 mmol) and malononitrile (**4**) (0.15 g, 2.2 mmol), and basic aluminum oxide (0.5 g) in anhydrous toluene (60 mL) was heated to 70 °C and stirred for 2h. The reaction mixture was then cooled to room temperature, and the basic aluminum oxide residue was removed by filtration and thoroughly washed with toluene. The solvent of the filtrate was removed by rotary evaporation, and the crude product was purified via column chromatography over SiO_2 with CH_2Cl_2 as the eluent. The product fractions were pooled, concentrated and further purified by recycling SEC ($CHCl_3$), yielding **CBM** (**8**) as a dark red solid (165 mg, 54%). ^{1}H NMR (700 MHz, $CDCl_3$): δ 8.94 (s, 2H), 8.91 (d, J = 7.0 Hz, 2H), 8.50 (s, 1H), 8.38 (d, J = 7.0 Hz, 1H), 8.35 (d, J = 7.0 Hz, 1H), 8.28 (s, 1H), 8.11 (d, J = 7.0 Hz, 2H) 7.92 (d, J = 7.0 Hz, 2H), 4.79 (m, 1H), 2.50-2.44 (m, 2H), 2.09-2.04 (m, 2H), 1.35-1.10 (m, 24H), 0.79 (t, J = 7.0 Hz, 6H), ^{13}C NMR (176 MHz, $CDCl_3$): δ 154.52, 153.16, 153.08, 143.15, 141.40, 141.30, 139.70, 134.10, 133.50, 130.75, 130.72, 127.66, 124.67, 123.35, 122.37, 121.35, 121.10, 120.66, 120.57, 113.79, 113.02, 110.99, 83.23, 56.90, 33.96, 31.77, 29.42, 29.36, 29.22, 26.87, 22.60, 14.07. HRMS (+APCI, m/z): calcd. for $C_{49}H_{47}N_9S_2$ $[M+H]^+$: 826.34294; found 826.34640.

2,2'-(4,4-dioctyl-4*H*-cyclo-penta[2,1-*b*:3,4-*b*']dithiophene-diyl)bis(benzo[*c*][1,2,5]thiadiazole-7,4-diyl))bis(methan-1-yl-1-ylidene)dimalononitrile (11, CDTBM): A mixture of 4,4-dioctyl-2,6-bis(trimethylstannanyl)-4*H*-cyclo-penta[2,1-*b*:3,4-*b'*]dithiophene **(9)** (0.128 g, 0.17 mmol), 4-Bromo-7-dicyanovinyl-2,1,3-benzothiadiazole **(10)** (0.1 g, 0.344 mmol) and $Pd(PPh_3)_4$ (5.9 mg, 0.03 eq) in a microwave vial was subjected to three vacuum/nitrogen cycles, and degassed toluene (3.0 ml) was added to the flask. The mixture was heated in a microwave reactor for 3 min at 120 °C, 3 min at 140 °C and 60 min at 175 °C. The solvent was removed and the residue was subjected to column chromatography using CH_2Cl_2/ethyl acetate (10/1) as the eluent. The product was further purified by recycling SEC ($CHCl_3$), yielding **CDTBM** (**11**) as a dark green solid (95 mg, 65%). ^{1}H NMR (700 MHz, $CDCl_3$): δ 8.82 (s, 2H), 8.81 (d, J = 7.0 Hz, 2H), 8.32 (s, 2H), 8.07 (d, J = 7.0 Hz, 2H), 2.09-2.06 (m, 4H), 1.28-1.18 (m, 20H), 1.11-1.07 (m, 4H), 0.81 (t, J = 7.0 Hz, 6H), ^{13}C NMR (176 MHz, $CDCl_3$): δ 161.95, 154.53, 152.02, 150.94, 142.90, 141.65, 133.79, 130.76, 125.04, 123.34, 121.20, 114.17, 113.42, 81.46, 54.65, 37.88, 31.80,

29.95, 29.33, 29.24, 24.72, 22.62, 14.09. HRMS (+APCI, m/z): calcd. for $C_{45}H_{42}N_8S_4$ $[M+H]^+$: 823.24488; found 823.24796.

3. Computational Analyses

All density functional theory (DFT) calculations were performed at the B3LYP/6-31G(d,p) level of theory with the Gaussian 09 (Revision C.01) software.[4] Side chains were modeled as methyl groups to reduce the computational cost. Although the side chains play an important role in the organization of small molecules and polymers in thin films, it is commonly assumed that the electronic properties of the single isolated small-molecule/polymer chain in the gas phase are well represented via this approach.[5-6]

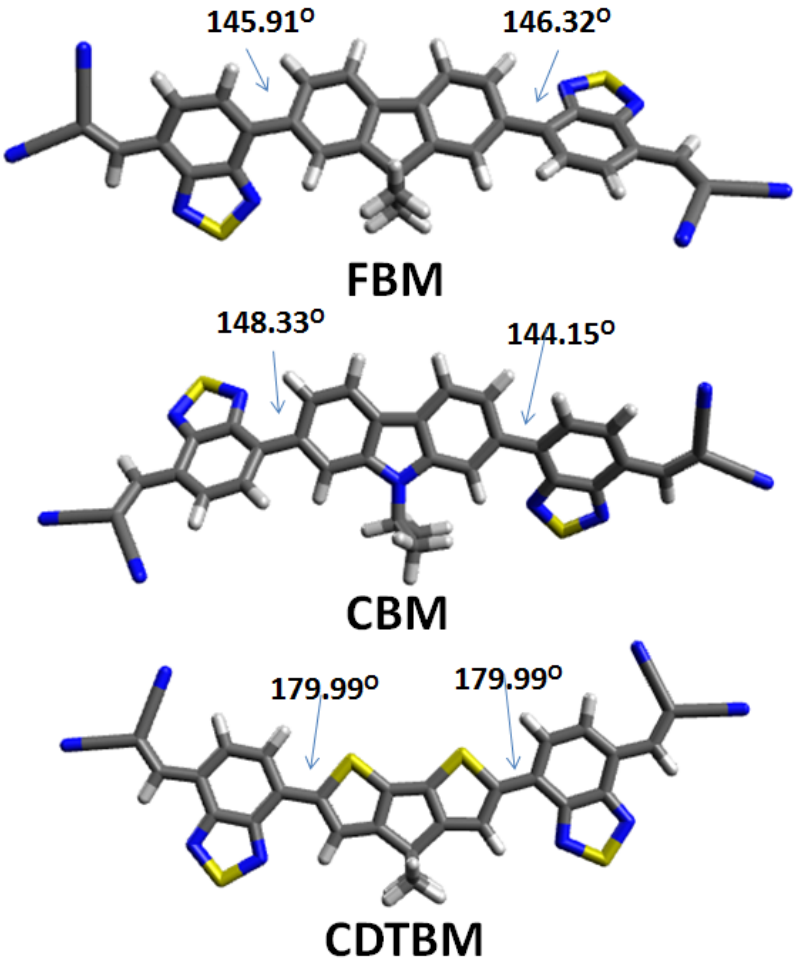

Figure S1. Optimized geometries and torsion angles for **FBM**, **CBM** and **CDTBM** obtained at the B3LYP/6-31G(d,p) level of theory.

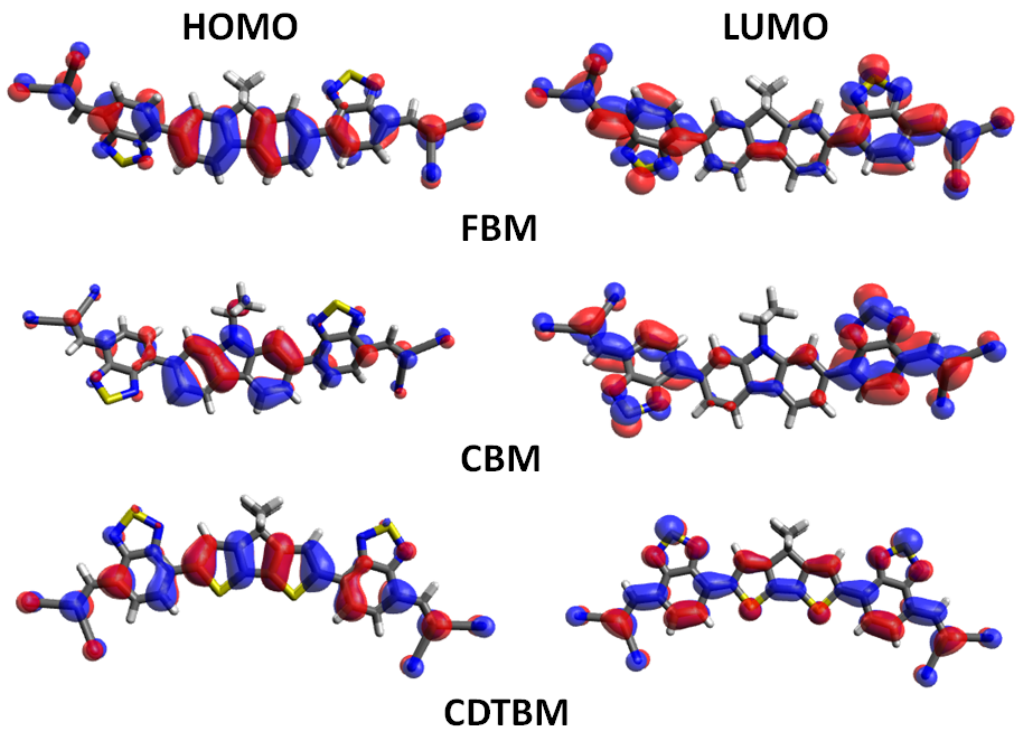

Figure S2. Representations of the LUMO and HOMO of **FBM**, **CBM** and **CDTBM** obtained at the B3LYP/6-31G(d,p) level of theory. The modeled frontier orbitals emphasize π-electron delocalization and localization effects across the SM acceptors.

4. UV-Vis Absorption

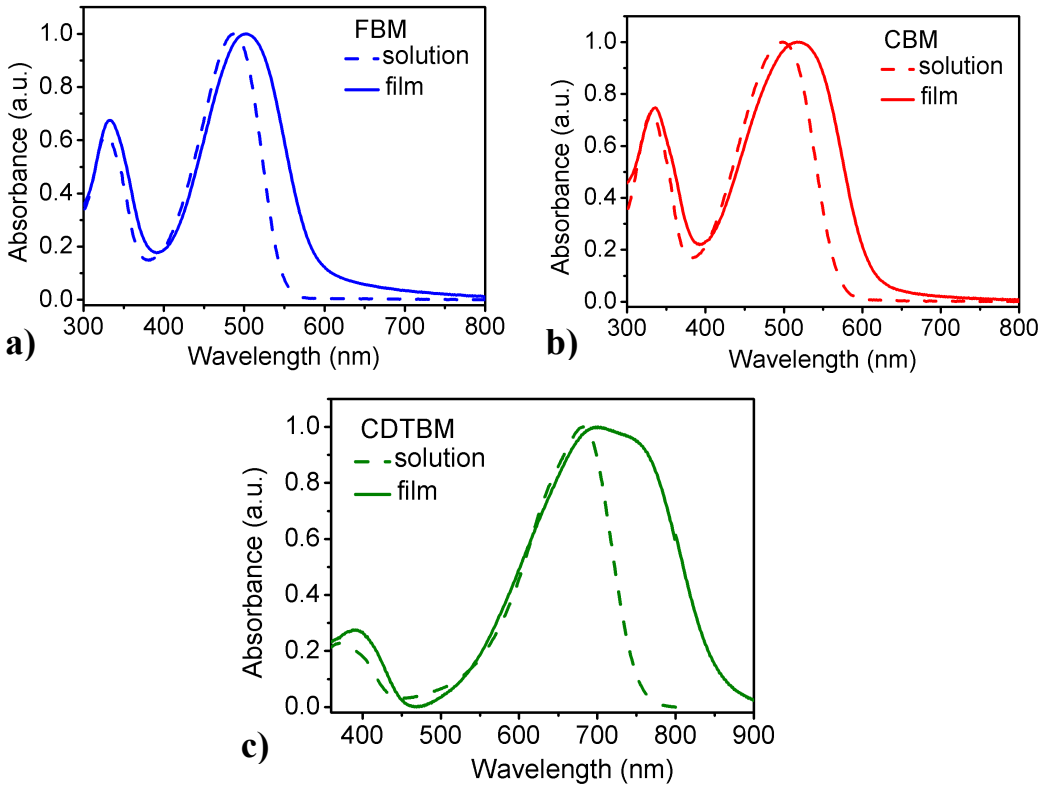

Figure S3. Normalized UV-Vis spectra of (a) **FBM**, (b) **CBM** and (c) **CDTBM** in chloroform solution (dotted curves) and for thin films cast from chlorobenzene onto glass substrates (solid curves).

5. Photoelectron Spectroscopy in Air (PESA) Measurements

Photoelectron spectroscopy in air (PESA) measurements were recorded using a Riken Keiki PESA spectrometer (Model AC-2) with a power setting of 10 nW and a power number of 0.33. Samples for PESA were prepared on glass substrates.

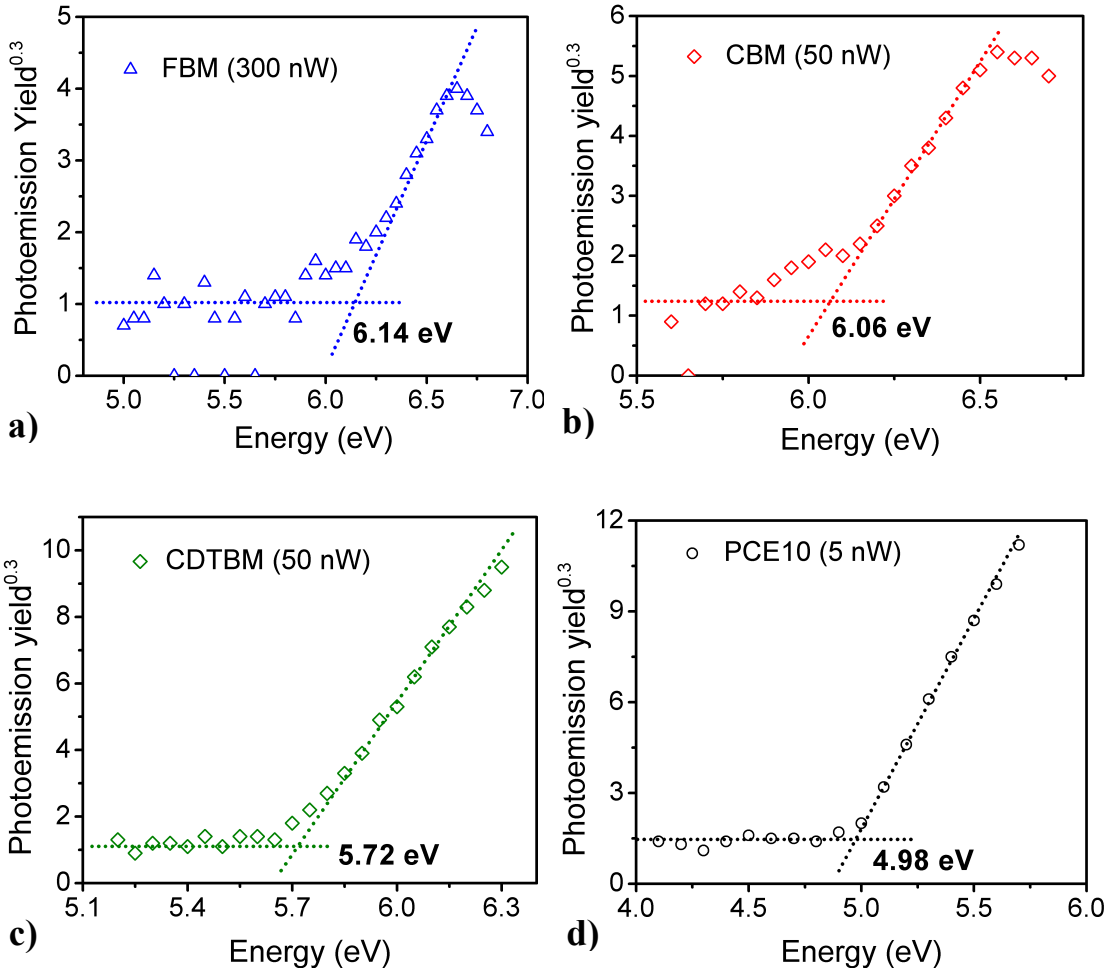

Figure S4. PESA curves for a) **FBM**, b) **CBM**, c) **CDTBM** and d) **PCE10**.

6. Cyclic Voltammetry (CV) Measurements

Electrochemical measurements were performed with a BAS 100W Bioanalytical electrochemical workstation, using Pt as working electrode, platinum wire as auxiliary electrode, and a porous glass wick Ag/Ag^+ as the pseudo-reference electrode standardized against ferrocene/ferrocenium (Fc/Fc^+); IP=$E_{onset,ox}$+5.1 eV and EA=$E_{onset,red}$+5.1 eV (absolute values). The oxidation onsets were measured in CH_2Cl_2 solutions and the reduction onsets were measured in DMF solutions containing 0.1 M of *n*-Bu_4NPF_6 as the supporting electrolyte, and using a scan rate of 100 mV s^{-1}. Fc/Fc^+ is taken to be 5.1 eV relative to the vacuum level.[7-8]

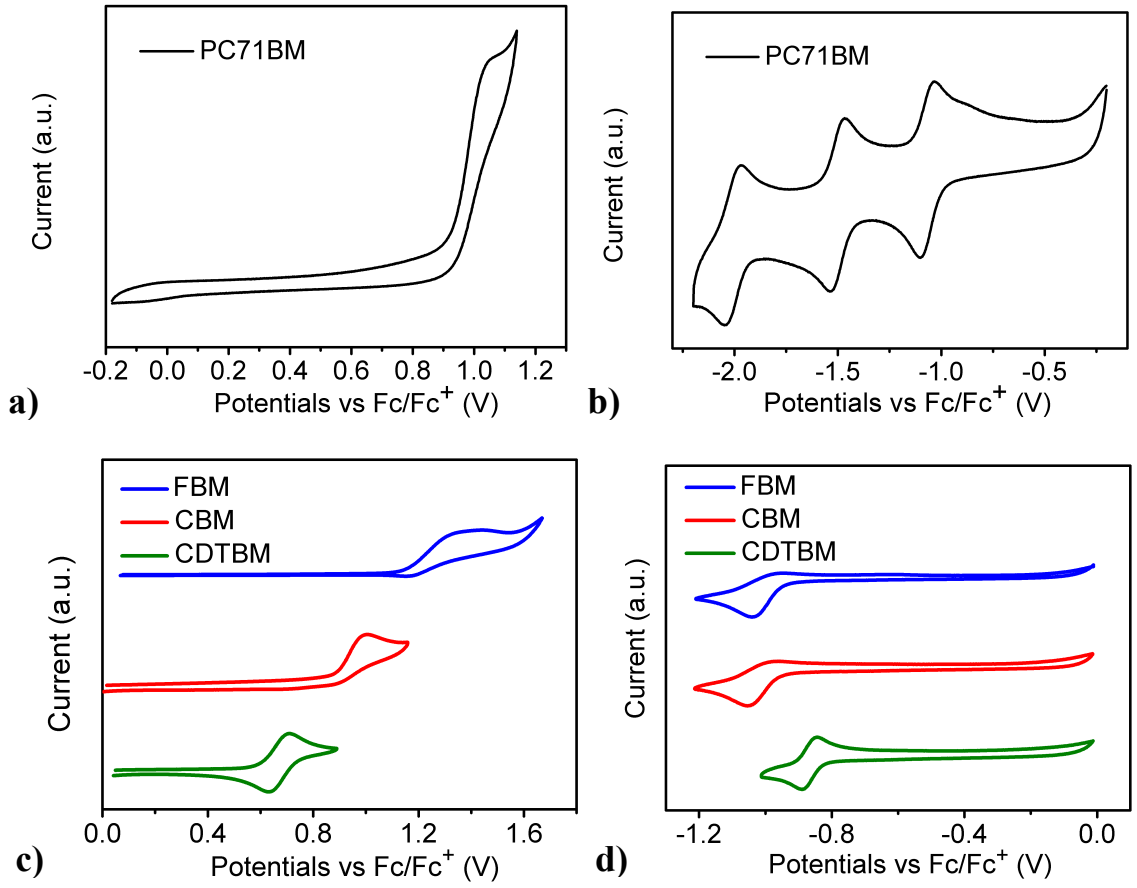

Figure S5. (a) Oxidation and (b) reduction cycles of $PC_{71}BM$ vs. Fc/Fc^+. (c) Oxidation and (d) reduction cycles of the SM acceptors **FBM**, **CBM**, and **CDTBM** vs. Fc/Fc^+.

7. Thermogravimetric Analyses (TGA)

Thermogravimetric analyses (TGA) were performed with a NETZSCH TG 209 F1 Iris under nitrogen atmosphere, with a set ramp rate of 10 K/min, and using Al_2O_3 (alox) crucibles.

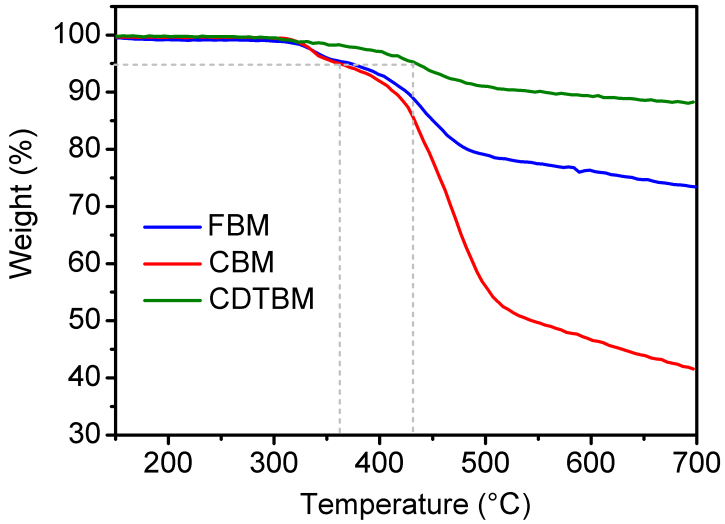

Figure S6. Thermogravimetric analyses (TGA) of **FBM**, **CBM** and **CDTBM**.

8. Differential Scanning Calorimetry (DSC)

Differential scanning calorimetry (DSC) analyses were performed with a NETZSCH DSC 204 F1 Phoenix under a nitrogen atmosphere, using aluminum crucibles.

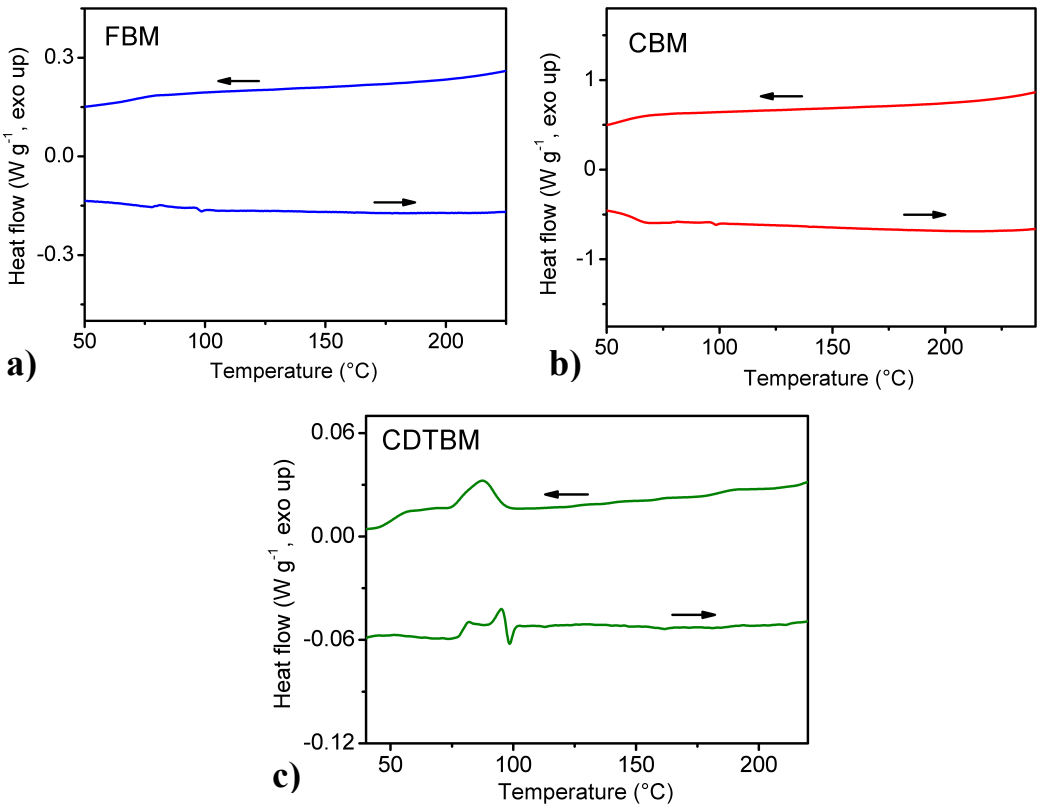

Figure S7. Differential scanning calorimetry (DSC) traces of 2nd cycle of a) **FBM**, b) **CBM** and c) **CDTBM**. Traces collected at a scan rate of 5 °C min^{-1} between 20 °C and 270 °C (temperatures converted and reported in °C on each plot); heating: bottom traces, cooling: upper traces.

9. Grazing Incidence Wide-Angle X-Ray Scattering (GIWAXS) Details

GIWAXS measurements were performed at the DELTA Synchrotron on beamline BL09. The beam size was 1.0 mm × 0.2 mm (width x height), and samples were irradiated just below the critical angle for total reflection with respect to the incoming X-ray beam (~0.1°); photon energy of 13 keV (λ = 0.9537 Å). The scattering intensity was detected on a 2D image plate (MAR-345) with a pixel size of 150 μm (2300 × 2300 pixels), and the detector was placed 523 mm from the sample center. All X-ray scattering measurements were performed under vacuum (~1mbar) to reduce air scattering and beam damage to the sample. All GIWAXS data were processed and analyzed with the software package Datasqueeze.

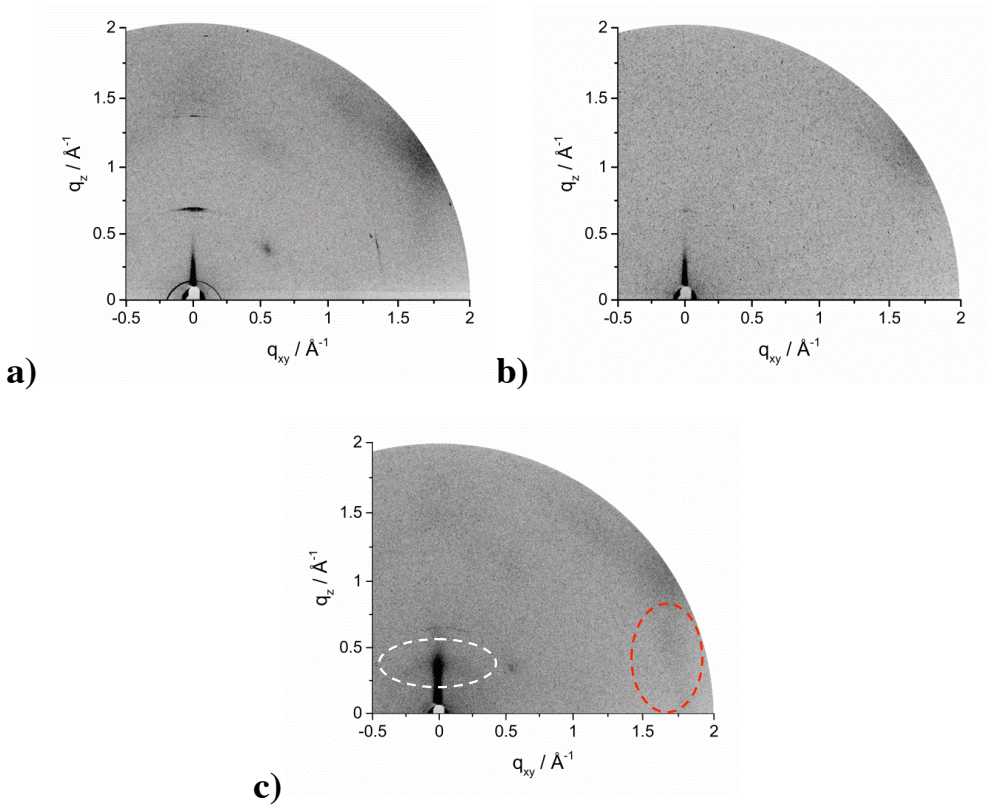

Figure S8. GIWAXS patterns of (a) **FBM**, (b) **CBM**, and (c) **CDTBM** in neat films cast from CB. In (a) and (b) the scattering intensities are parasitic and pertain to the substrate (Si wafer); the GIWAXS patterns of the films of **FBM** and **CBM** do not show any reflections characteristic of π-stacking, and lack higher-order reflections characteristic of long-range ordering. In (c) the scattering peak intensity along q_z (0.2-0.5 Å^{-1}, circled white, interlayer peak) and the weak π-stacking reflection centered along q_{xy} (ca. 1.75 Å^{-1}, circled red) suggest the presence of edge-on-

oriented aggregates in films of **CDTBM;** in-plane π-stacking peak: 0.35 nm; out-of-plane interlayer spacing: 1.50 nm.

10. Device fabrication

The solar cells were prepared on glass substrates with tin-doped indium oxide (ITO, 15 Ω sq^{-1}) patterned on the surface. Substrates were first scrubbed with isopropanol to remove organic residues before immersing in an ultrasonic bath of dilute Extran 300 for 15 min. Samples were rinsed in flowing deionized water for 5 min before being sonicated (Branson 5510) for 15 min each in successive baths of deionized water, acetone and isopropanol. Next, the samples were dried with pressurized nitrogen before being exposed to an UV−ozone plasma for 15 min. In parallel, a precursor solution of zinc acetate dihydrate (200 mg), 2-methoxyethanol (4 ml), and ethanolamine (55 µl) was prepared and stirred vigorously in air for at least 12h. This resulting precursor solution was spun-cast at 3000 rpm onto the cleaned ITO substrates, affording smooth amorphous ZnO thin films (*a*-ZnO) (serving as electron transport/extraction layers; detailed synthesis and method described in our prior published work[9]), which were then baked at 150°C for 20 min. Immediately after baking the *a*-ZnO-coated substrates, the samples were transferred into a dry nitrogen glovebox (< 3 ppm O_2) for active layer deposition.

All solutions were prepared in the glovebox using the polymer PCE10 (purchased from 1-Material) and the SM acceptors **FBM**, **CBM** and **CDTBM**. PCE10 and the SM acceptors were dissolved in chlorobenzene, and the solutions were stirred for at least 2h at 50°C. Optimized devices were prepared using solution blends of 20 mg mL^{-1} concentration, a PCE10:SM ratio of 4:6 (by weight) for PCE10:**FBM** and **CDTBM**, and a PCE10:SM ratio of 3:7 (by weight) for PCE10:**CBM**. The effects of different blend ratios and additive concentrations on device performance were also examined. The active layers were spun-cast from the solutions at 50°C at an optimized spin speed of 2000 rpm for 30 s, using a programmable spin coater from Specialty Coating Systems (Model G3P-8), resulting in a film of *ca.* 70 nm in thickness. The samples were then dried under vacuum for at least 1 hour. Next, the samples were placed in a thermal evaporator for evaporation of a 5 nm thick molybdenium oxide (MoO_3) layer evaporated at 0.5 Å s^{-1}, and a 100 nm thick layer of silver evaporated at 5 Å s^{-1}; pressure of less than $2x10^{-6}$ Torr. Following electrode deposition, samples underwent *J-V* testing.

J-V measurements of solar cells were performed in the glovebox with a Keithley 2400 source meter and an Oriel Sol3A Class AAA solar simulator calibrated to 1 sun, AM1.5 G, with a KG-5 silicon reference cell certified by Newport. The external quantum efficiency (EQE) measurements were performed at zero bias by illuminating the device with monochromatic light supplied from a Xenon arc lamp in combination with a dual-grating monochromator. The number of photons incident on the sample was calculated for each wavelength by using a silicon photodiode calibrated by NIST.

11. Additional PV Device Performance Data

Table S1. Summary of average PV performance for PCE10:**FBM**, PCE10:**CBM** and PCE10:**CDTBM** active layers cast from different donor/acceptor (D/A) ratios.

Acceptors	D/A Ratio	V_{OC} [V]	J_{SC} [mA/cm^2]	FF [%]	Avg. PCE [%]
FBM	6:4	0.86±0.01	5.9±0.2	31±0.6	1.6±0.04
	5:5	0.86±0.03	9.8±0.4	36±2	3.0±0.3
	4:6	0.88±0.01	10.8±0.5	44±2	4.2±0.1
CBM	5:5	0.75±0.04	8.5±0.1	38±0.9	2.5±0.2
	4:6	0.85±0.02	9.7±0.2	40±2	3.3±0.2
	3:7	0.89±0.01	9.4±0.4	48±2	4.0±0.1
	2:8	0.88±0.02	6.0±0.1	56±1	3.0±0.03
CDTBM	6:4	0.68±0.01	7.9±0.1	39±1	2.1±0.1
	5:5	0.68±0.01	11.5±0.1	44±0.6	3.4±0.1
	4:6	0.68±0.01	11.7±0.2	53±2	4.2±0.2
	3:7	0.66±0.01	11.0±0.1	56±2	4.1±0.2

Table S2. Summary of average PV performance for PCE10:**FBM**, PCE10:**CBM** and PCE10:**CDTBM** active layers cast from an optimized D/A ratio and using different concentration of solution-processing additive (CN or DIO).

Acceptors	vol% additive	V_{OC} [V]	J_{SC} [mA/cm^2]	FF [%]	Avg. PCE [%]
FBM (4:6, CN)	0.8	0.88±0.01	10.5±0.1	52±1	4.8±0.03
	1	0.88±0.01	11.2±0.5	51±2	5.0±0.05
	1.4	0.87±0.003	11.7±0.05	48±1	4.9±0.13
	1.8	0.86±0.01	11.6±0.02	46±4	4.6±0.5
CBM (3:7, DIO)	0.4	0.89±0.01	9.5±0.2	53±4	4.4±0.2
	1	0.88±0.003	9.8±0.2	52±0.7	4.5±0.05
	1.5	0.88±0.005	10.2±0.7	51±3	4.6±0.05
	2	0.88±0.005	10.6±0.7	53±3	5.0±0.2
CDTBM (4:6, CN)	0.3	0.66±0.01	12.4±0.1	53±4	4.3±0.4
	0.5	0.65±0.01	12.4±0.2	54±4	4.4±0.5
	0.8	0.66±0.01	11.9±0.6	60±3	4.8±0.1
	1	0.68±0.003	11.9±0.1	52±2	4.2±0.2

12. BHJ Thin-Film Absorption

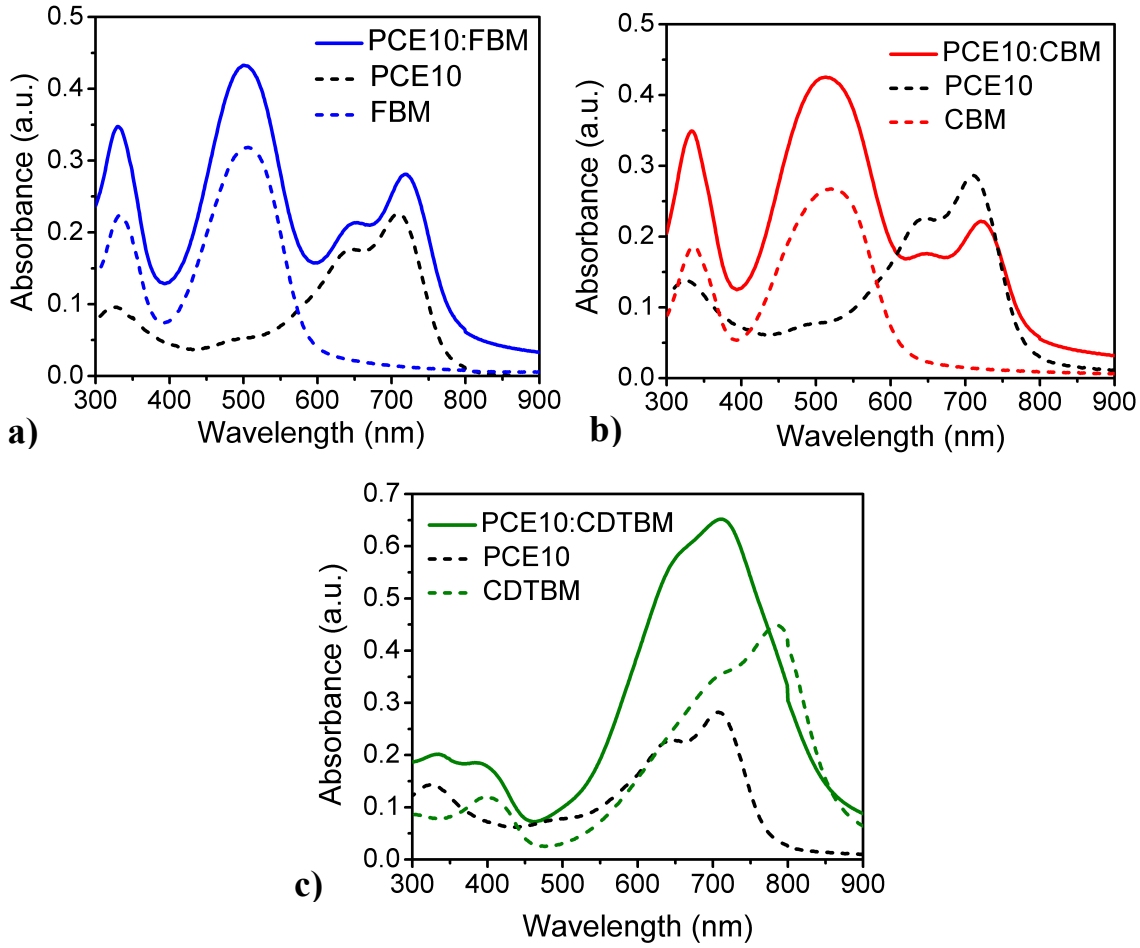

Figure S9. Normalized thin-film absorption spectra of (a) **FBM**, PCE10, and a PCE10:**FBM** blend film (4:6 w/w), (b) **CBM**, PCE10, and a PCE10:**CBM** blend film (3:7 w/w), and (c) **CDTBM**, PCE10, and a PCE10:**CDTBM** blend film (4:6 w/w).

13. J_{SC} Modeling via Transfer Matrix

Transfer matrix modeling[10] was used to simulate maximum theoretical J_{SC} plots as a function of active layer thickness (thickness range: 0-400 nm) for optimized blends of PCE10:**FBM**, PCE10:**CBM**, and PCE10:**CDTBM**; the model assumes 100% internal quantum efficiency (IQE). The transfer matrix code used for these simulations was developed by George F. Burkhard and Eric T. Hoke; code available from: http://web.stanford.edu/group/mcgehee/

transfermatrix/index.html. The active layers optical constants n and k were collected via multi-sample analysis by variable angle spectroscopic ellipsometry (VASE) with an M-2000 ellipsometer (J.A. Woolam Co., Inc). The active layers were cast on clean silicon substrates with different thicknesses of SiO_2 (25 nm, 51 nm, 70 nm and 115 nm) according to the device casting conditions described earlier in Section 10. Device Fabrication. The VASE measurements were performed with incident angles being varied from 45 to 75° in steps of 10° relative to the samples. The software Complete Ease (J.A. Woolam Co., Inc) was used to process all collected data, and the optical constants n and k were inferred from the B-splines[11] model.

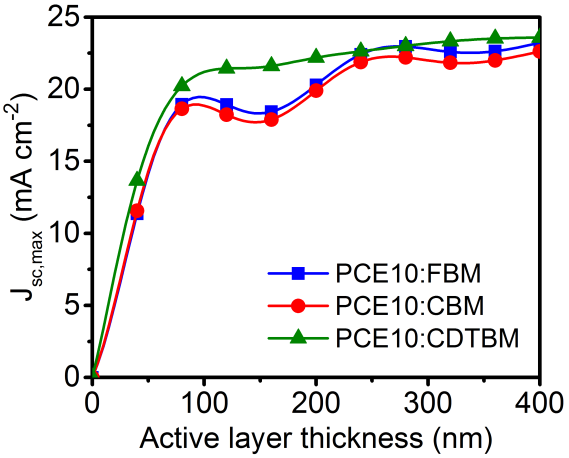

Figure S10. Maximum theoretical J_{SC} plots as a function of active layer thickness simulated via transfer matrix for optimized blends of PCE10:**FBM**, PCE10:**CBM**, and PCE10:**CDTBM**; the model assumes 100% IQE.

14. Transmission Electron Microscopy (TEM) Imaging

Films of ca. 70 nm thickness were spun-cast on PEDOT:PSS-coated glass substrates. The PCE10:SM BHJ films were floated off the PEDOT:PSS-coated substrates in deionized water and collected on lacey carbon coated TEM grids (Electron Microscopy Sciences). TEM images were recorded in bright field mode with a microscope operating at 120 keV (Tecnai Bio twin, FEI), using an 4k x 4k eagle CCD camera (FEI).

15. Atomic Force Microscopy (AFM) Imaging

A Dimension Icon atomic force microscope (AFM) from Bruker was used to image the active layers in tapping mode (heights and phase images are represented below).

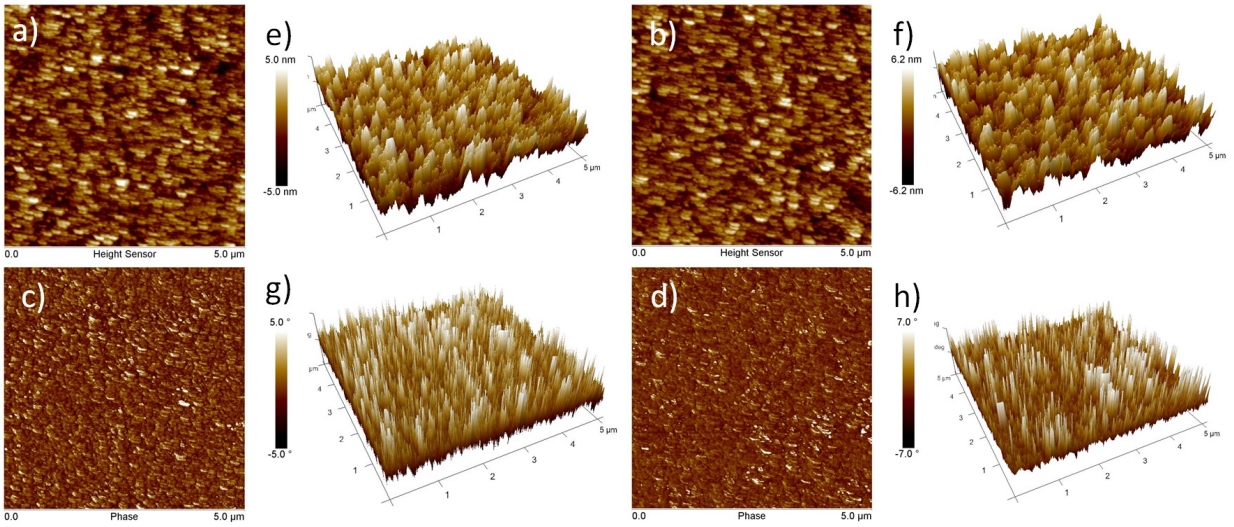

Figure S11. (a,b) AFM height, (c,d) phase images and (e-f) 3D images of 5 x 5 μm^2 for PCE10:**FBM** (4:6, w/w) active layers. (a,c,e,g) without additive, root-mean-square (RMS) roughness: 1.35 nm, and (b,d,f,h) with 1% CN, RMS roughness: 2.99 nm.

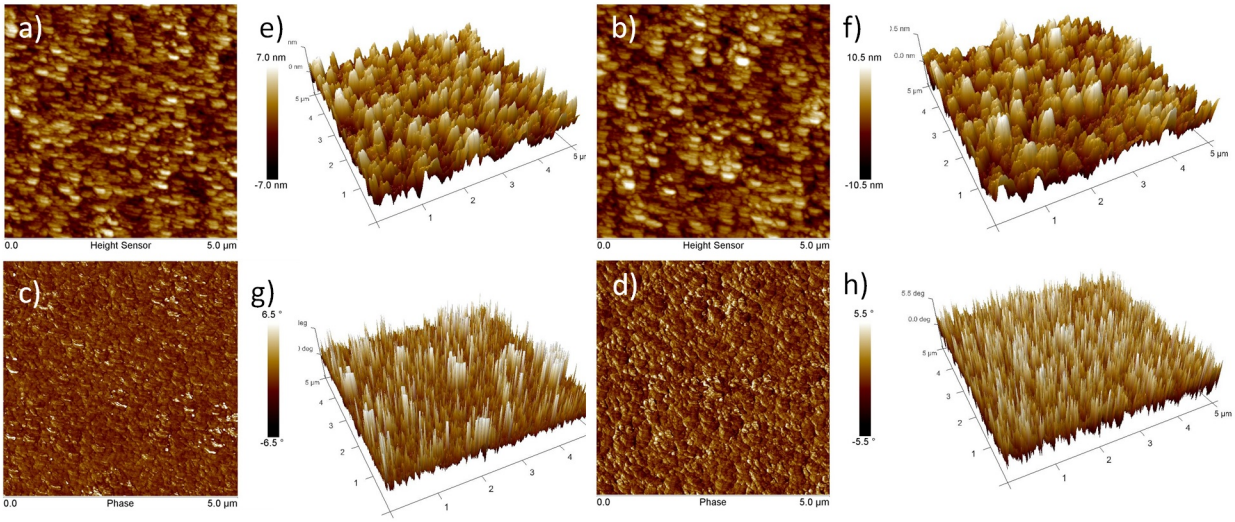

Figure S12. (a,b) AFM height, (c,d) phase images and (e-f) 3D images of 5 x 5 μm^2 for PCE10:**CBM** (4:6, w/w) active layers. (a,c,e,g) without additive, RMS roughness: 2.21 nm, and (b,d,f,h) with 3% DIO, RMS roughness: 2.81 nm.

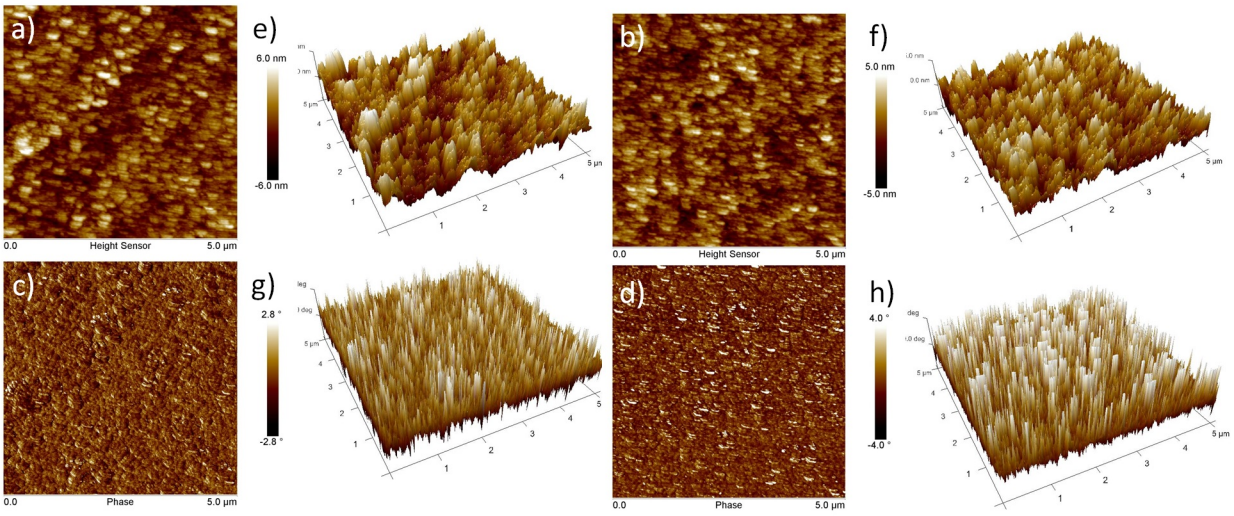

Figure S13. (a,b) AFM height, (c,d) phase images and (e-f) 3D images of 5 x 5 μm^2 for PCE10:**CDTBM** (3:7, w/w) active layers, (a,c,e,g) without additive, RMS roughness: 2.97 nm, and (b,d,f,h) with 0.8% CN, RMS roughness: 1.18 nm.

16. Photoluminescence (PL) Quenching

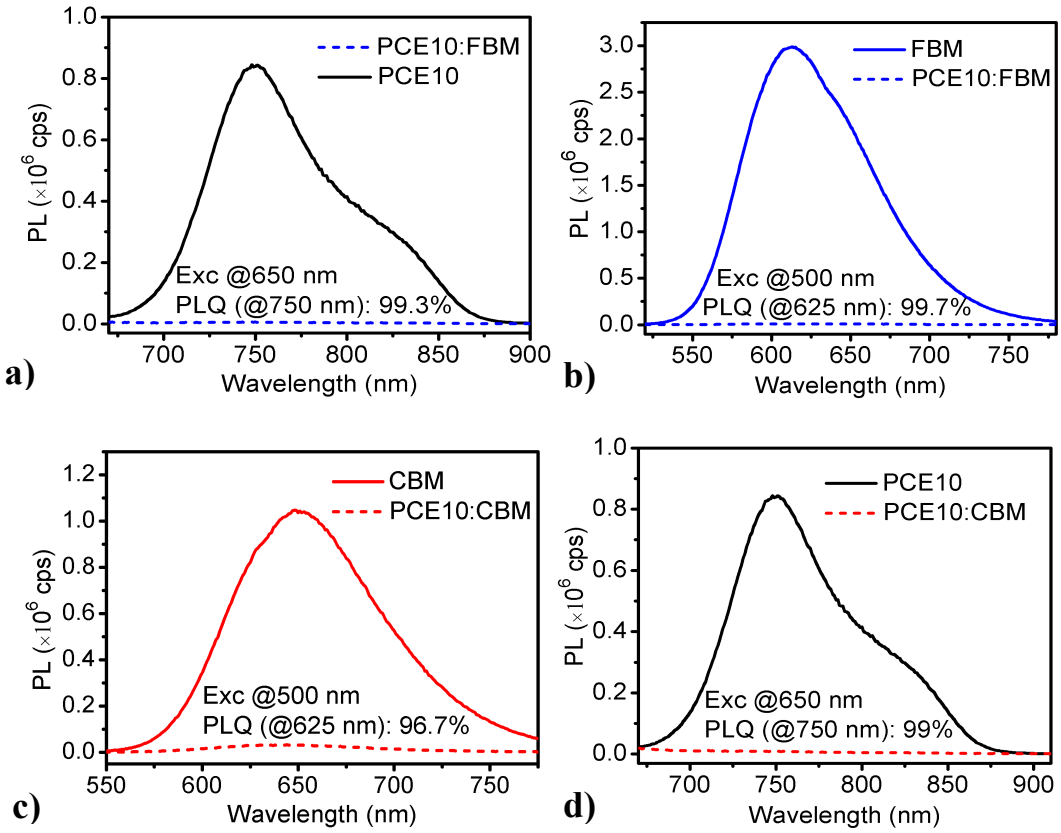

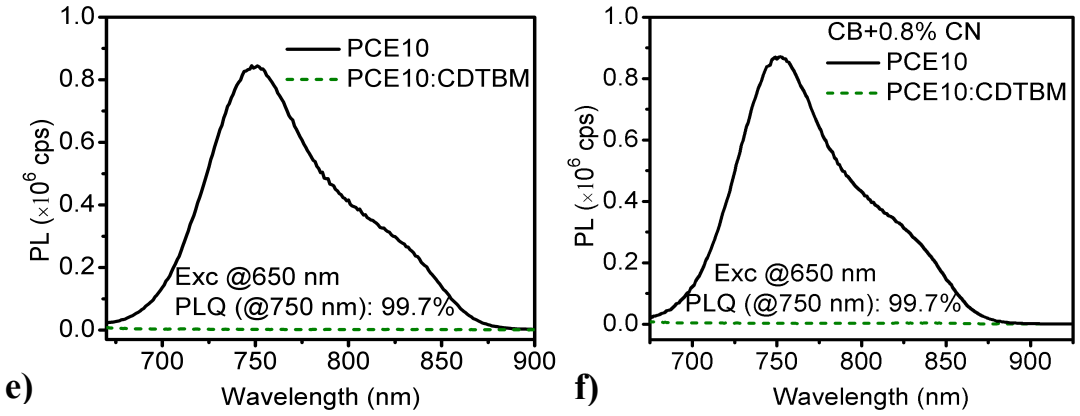

Figure S14. Photoluminescence (PL) quenching of PCE10 and the SM acceptor analogues **FBM** and **CBM** in neat films without additive (solid lines), and in the presence of the donor/acceptor counterpart (dashed lines) as in BHJ thin films; **(a)** PCE10:**FBM**, without additive, excitation at 500 nm, **(b)** PCE10:**FBM** without additive, excitation at 650 nm, **(c)** PCE10:**CBM**, without additive, excitation at 500 nm, **(d)** PCE10:**CBM**, without additive, excitation at 650 nm, **(e)** PCE10:**CDTBM**, without additive, excitation at 650 nm, **(f)** PCE10:**CDTBM** with additive, excitation at 650 nm.

17. Additional GIWAXS Details

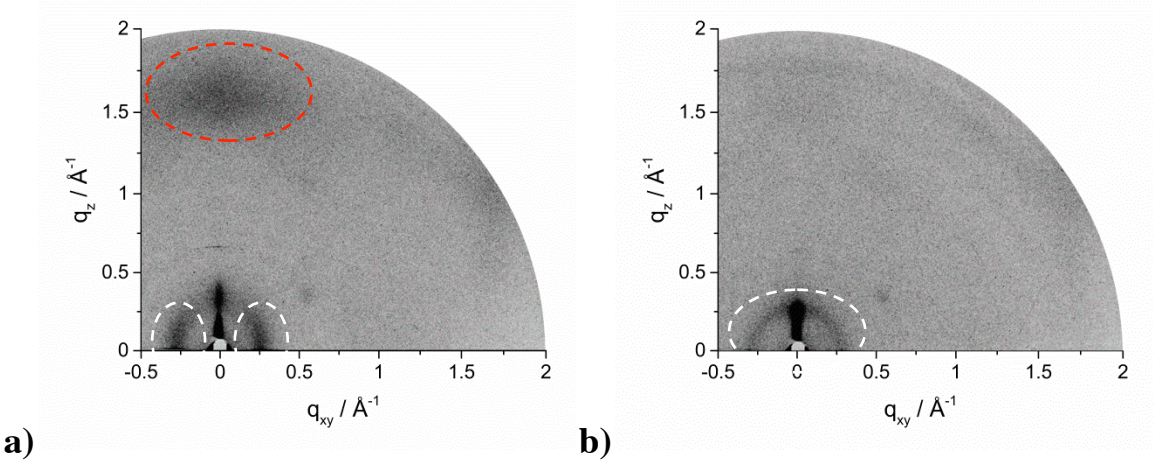

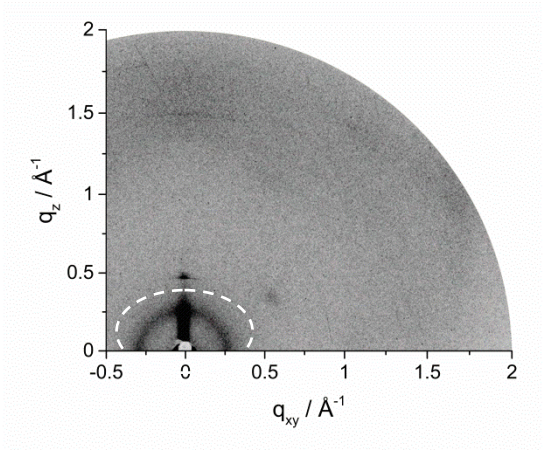

c)

Figure S15. GIWAXS patterns of (a) PCE10, (b) PCE10:**CDTBM** cast from CB and (c) PCE10:**FBM** cast from CB+1%CN. Red circles point to π-stacking reflections and white ones are related to interlayer peaks; unmarked reflections arise from substrate scattering. We note that PCE10 aggregates adopt preferential face-on orientations in neat films as indicated by (i) the broad wide-angle out-of-plane reflection (circled red in Fig. S15a) which points to relatively pronounced π-stacking correlations (π-π stacking distance of *ca.* 0.39 nm), and (ii) the small-angle in-plane scattering intensity characteristic of lamellar stacking (d-spacings of 2.27 nm). The GIWAXS plots of all PCE10:SM blend films showed the same common pattern (see PCE10:**CDTBM** in Fig. S15b) consisting of a single/main reflection attributed to the polymer lamellar stacking (ca. 2.10 nm in PCE10:**CDTBM**) with two contributions: one main out-of-plane peak characteristic of edge-on-oriented aggregates and a secondary isotropic reflection/ring characteristic of randomly-oriented aggregates. The comparable ordering patterns of all PCE10:SM blend films is consistent with the comparable solar cell performance of all active layers. Using CN or DIO additives in the solution-casting process did not change the overall aggregation pattern and lack of long-range order in the blend films of PCE10 and the SM acceptors (see PCE10:**FBM** in Fig. S15c, but led to a slight increase in the polymer interlayer spacing to 2.24 nm in PCE10:**FBM** and PCE10:**CBM**, and to 2.14 nm in PCE10:**CDTBM**.

18. Carrier Mobility Measurements

The carrier mobilities (hole and electron mobilities) of optimized BHJ films with PCE10 and the SM acceptors were determined by fitting the dark currents of hole/electron-only diodes to the space-charge-limited current (SCLC) model. *Hole-only diode configuration*: Glass/ITO/PEDOT /BHJ/MoO_3/Ag. First, a thin layer (*ca.* 30 nm) of PEDOT:PSS was spin-coated at 4000 rpm for 30 s onto the ITO-coated glass in air and then baked at 150º C for 10 min. After deposition of the active layer on the PEDOT:PSS-coated substrates, MoO_3 (5 nm, 0.3 Å s^{-1}) and Ag (100 nm, 5 Å s^{-1}) were deposited via thermal evaporation in a vacuum chamber at a base pressure of 2×10^{-6} mbar. *Electron-only diode configuration*: Glass/ITO/*a*-ZnO/PFN-Ox[12]/BHJ/Ca/Ag. Amorphous ZnO layers were prepared as described in Section 10. Device Fabrication. A solution of 0.5 mg mL^{-1} PFN-Ox in methanol:acetic acid (100:1 v/v) was spun-cast at 2000 rpm onto the ZnO/ITO-coated substrates to yield a *ca.* 5 nm interlayer, which was then heated and cross-linked at 150 °C for 20 min. The active layers were then deposited on top of the PFN-Ox/ZnO/ITO-coated substrates, and calcium (7 nm, 0.4 Å s^{-1}) and Al (100 nm, 5 Å s^{-1}) were subsequently deposited via thermal evaporation in a vacuum chamber at a base pressure of less than 2×10^{-6} mbar. Active-layer thicknesses were measured with a Tencor surface profilometer.

The carrier mobilities were inferred from fitting the data to the Murgatroyd expression:[13]

$$J(V) = \frac{9}{8}\varepsilon_0\varepsilon_r\mu_0 \exp\left(0.89\beta\sqrt{\frac{V-V_{bi}}{L}}\right)\frac{(V-V_{bi})^2}{L^3}$$

Definition	Variable	Units
zero-field mobility	μ_0	$cm^2\ V^{-1}\ s^{-1}$
film thickness	L	cm
dark current density	J	$A\ cm^{-2}$
voltage	V	V
vacuum permittivity	ε_0 (8.854×10^{-14})	$A\ s\ V^{-1}\ cm^{-1}$
dielectric constant	ε_r (3.3)	-
field activation factor	β	$cm^{1/2}\ V^{-1/2}$

Table S3. Carrier mobilities for BHJ thin films of **FBM**, **CBM**, **CDTBM** and $PC_{71}BM$ acceptors blended with the polymer donor PCE10.

Acceptors	$\mu_{0,h}$ ($cm^2V^{-1}s^{-1}$)	$\mu_{0,e}$ ($cm^2V^{-1}s^{-1}$)	β_e ($cmV^{-1})^{1/2}$
FBM (CB+1%CN)	$(1.4\pm0.1) \times 10^{-4}$	$(1.0\pm0.3) \times 10^{-6}$	$(3.6\pm0.4) \times 10^{-3}$
CBM (CB+2%DIO)	$(1.0\pm0.3) \times 10^{-4}$	$(1.9\pm0.5) \times 10^{-6}$	$(4.2\pm0.6) \times 10^{-3}$
CDTBM (CB+0.8%CN)	$(3.4\pm1.0) \times 10^{-4}$	$(1.8\pm0.4) \times 10^{-6}$	$(2.6\pm0.3) \times 10^{-3}$
$PC_{71}BM$ (CB)	$(7.3\pm2.0) \times 10^{-4}$	$(1.5\pm0.8) \times 10^{-4}$	$(4.9\pm2.6) \times 10^{-4}$

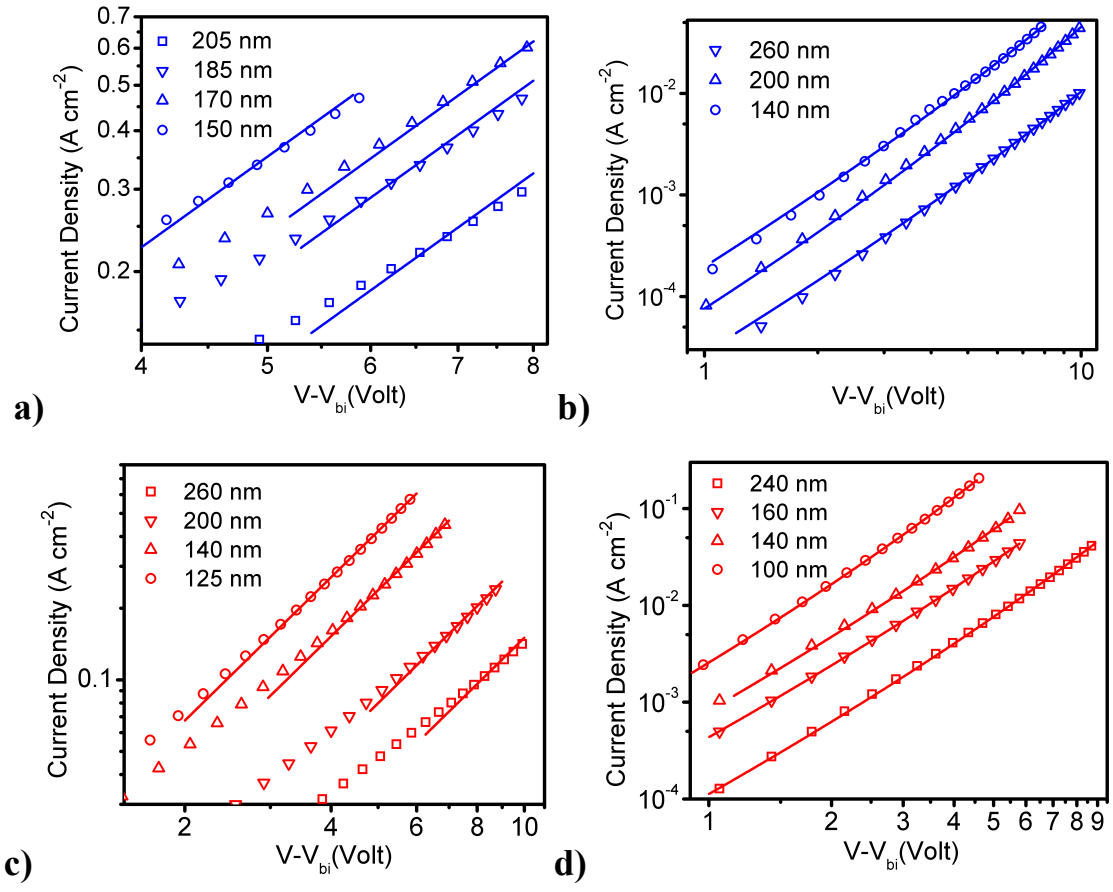

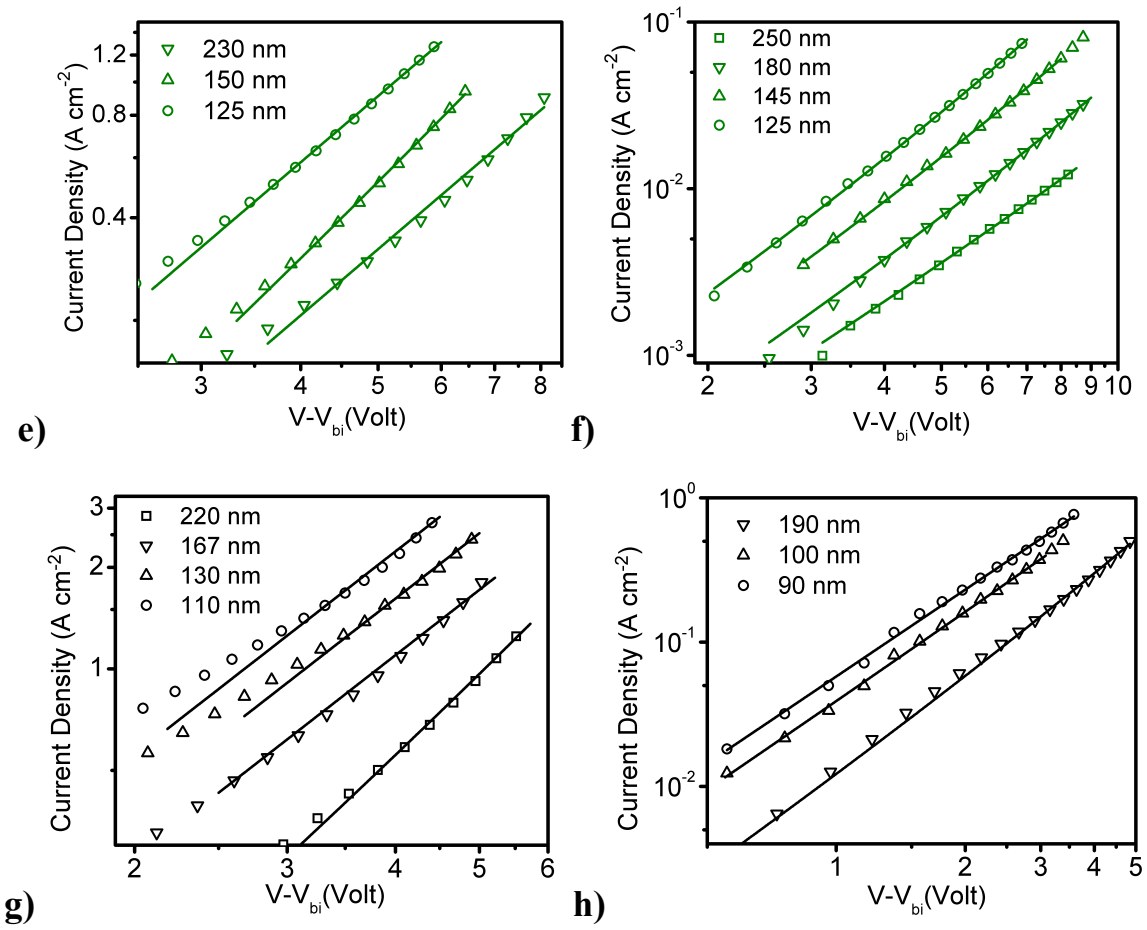

Figure S16. Dark *J–V* curves of PCE10:SM and PCE10:$PC_{71}BM$ BHJ thin films of various thicknesses: a) hole-only diodes, b) electron-only diodes based on PCE10:**FBM** (4:6 with 1% CN), c) hole-only diodes, d) electron-only diodes based on PCE10:**CBM** (3:7 with 2% DIO), e) hole-only diodes, f) electron-only diodes based on PCE10:**CDTBM** (4:6 with 0.8% CN), g) hole-only diodes, h) electron-only diodes based on PCE10:$PC_{71}BM$. The hole-only device structure is Glass/ITO/PEDOT/BHJ/MoO_3/Ag; here, V_{bi} = 0 (flat band pattern formed by PEDOT-MoO_3) and, as a result $V_{in} = V - V_{bi} = V$. The electron-only device structure is Glass/ITO/*a*-ZnO/PFN-Ox/BHJ/Ca/Ag; here, V_{bi} = 0.4 V. The solid lines are fits to the experimental data according to the Murgatroyd expression.

19. Solution NMR Spectra

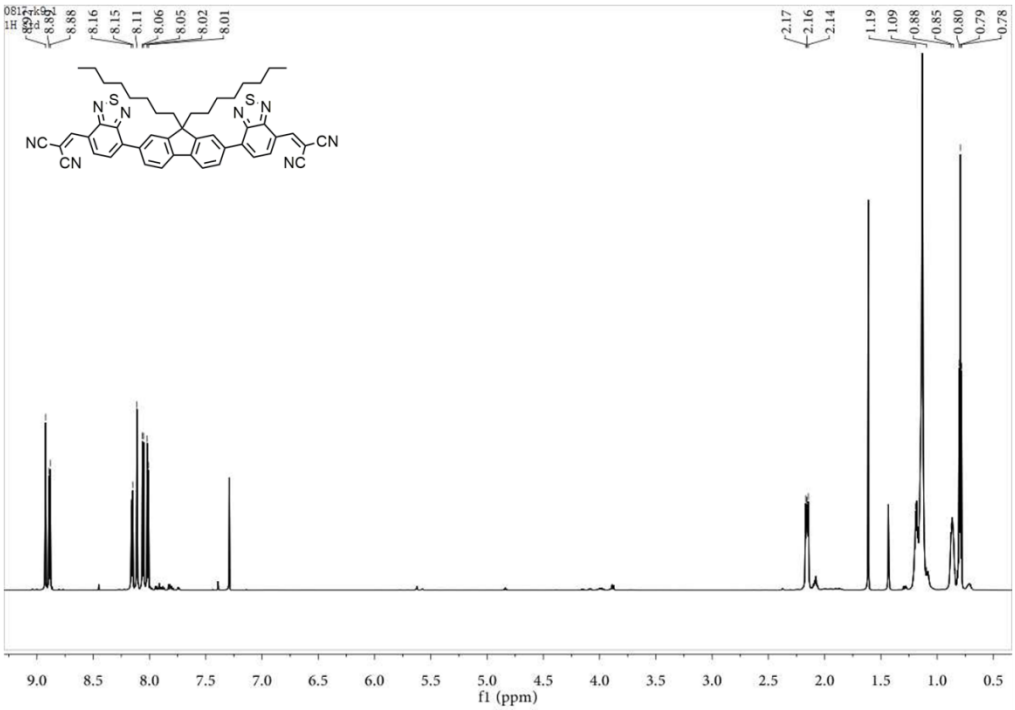

Figure S17. ^{1}H NMR spectrum of **FBM**.

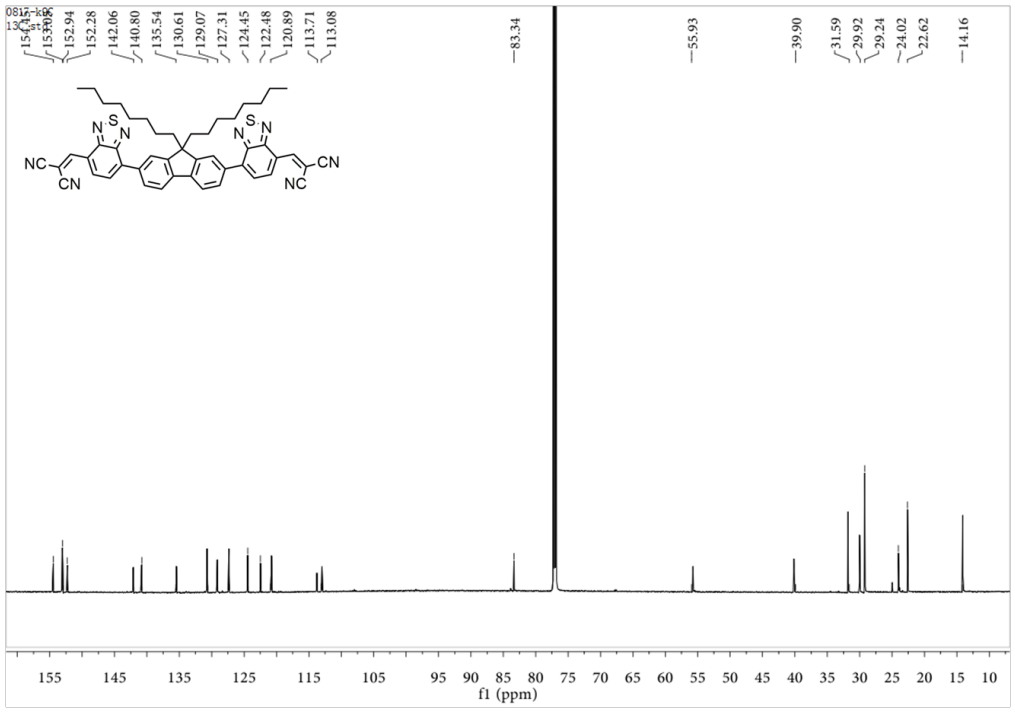

Figure S18. ^{13}C NMR spectrum of **FBM**.

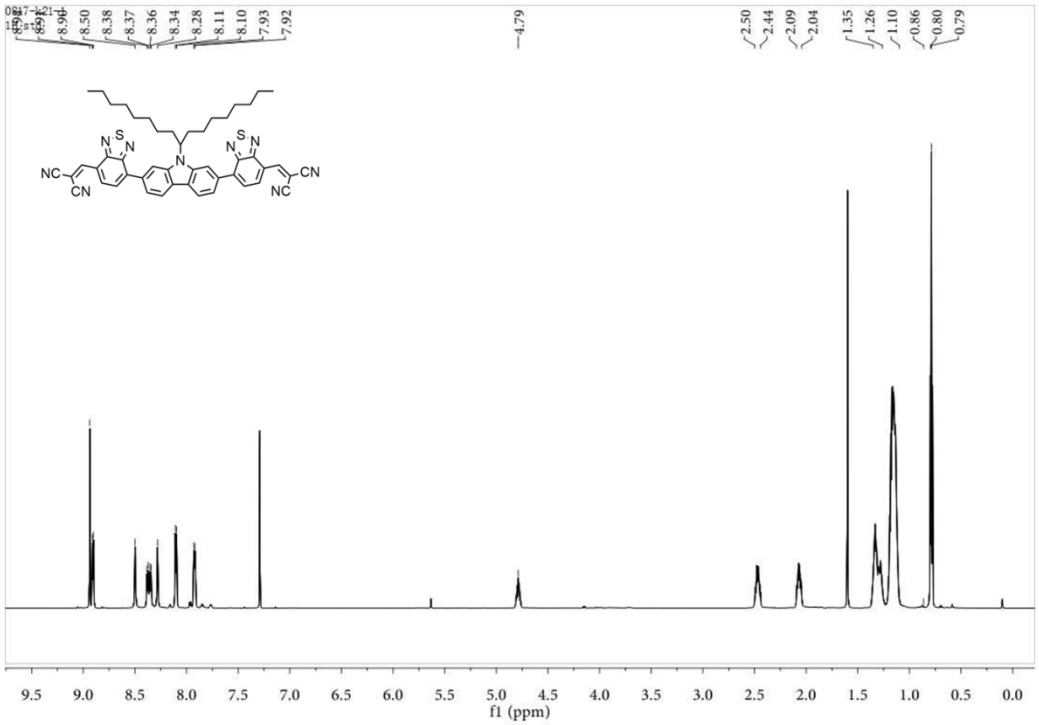

Figure S19. ^{1}H NMR spectrum of **CBM**.

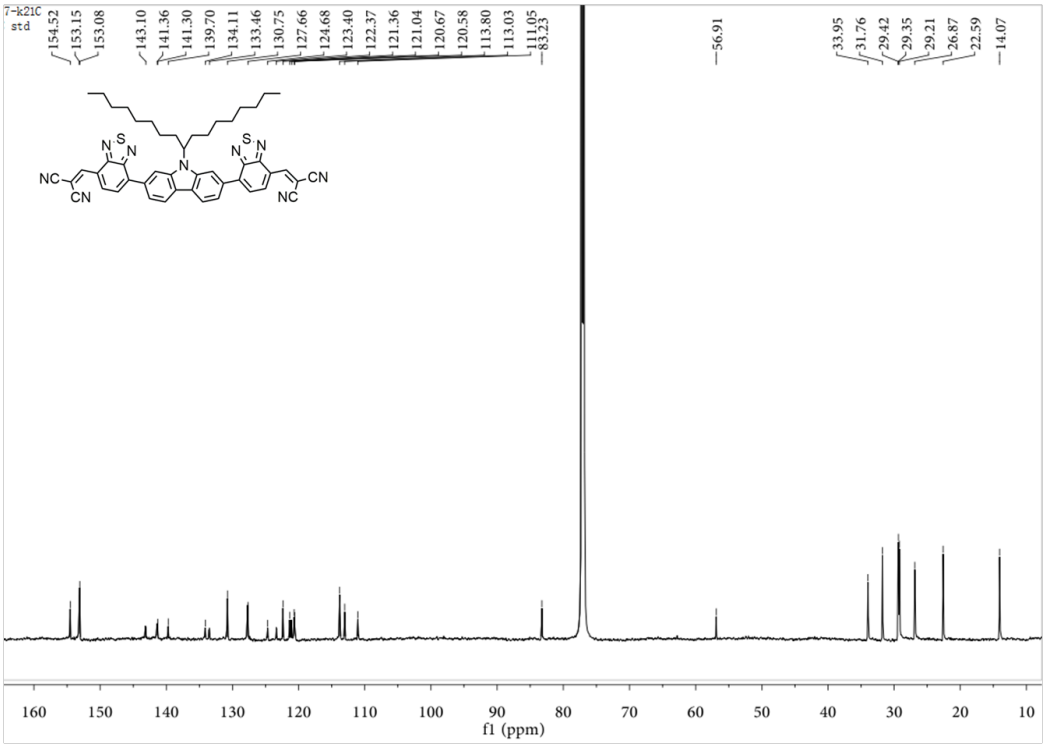

Figure S20. ^{13}C NMR spectrum of **CBM**.

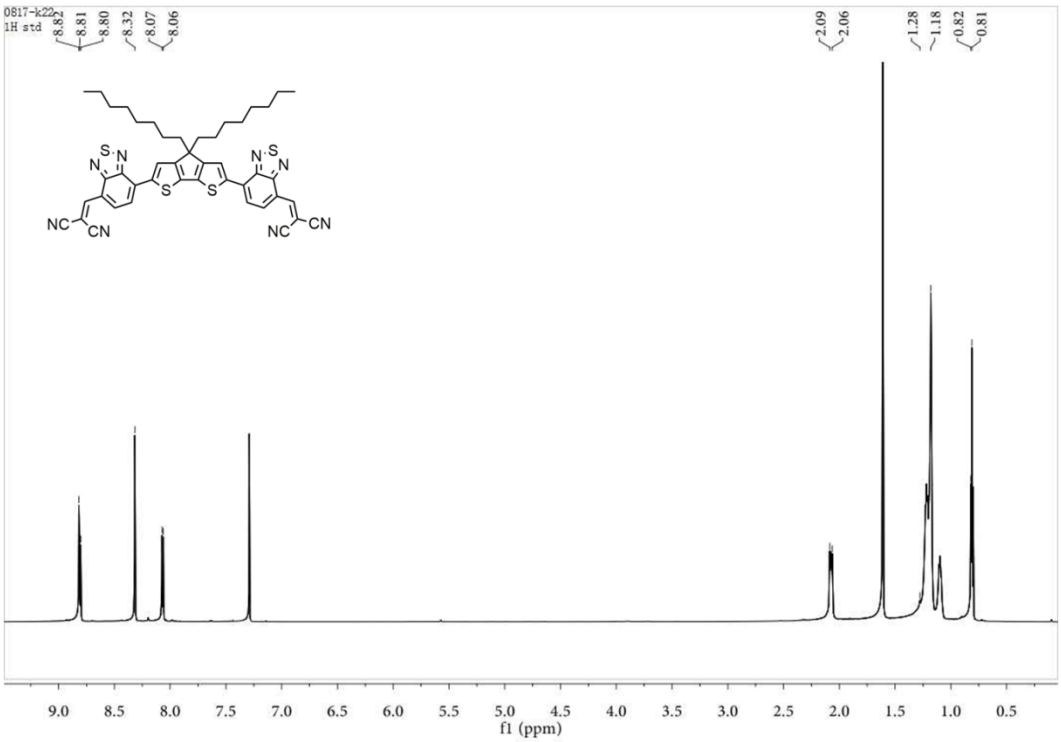

Figure S21. ^{1}H NMR spectrum of **CDTBM**.

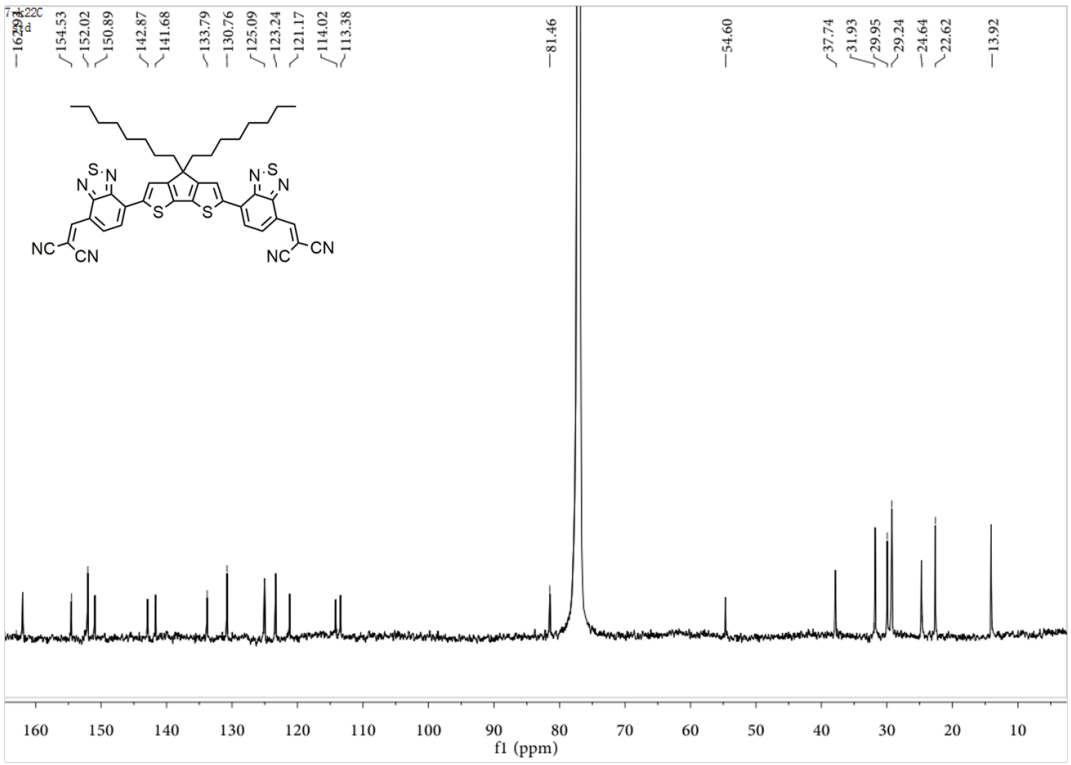

Figure S22. ^{13}C NMR spectrum of **CDTBM**.

20. References

(1) Lin, L.-Y.; Chen, Y.-H.; Huang, Z.-Y.; Lin, H.-W.; Chou, S.-H.; Lin, F.; Chen, C.-W.; Liu, Y.-H.; Wong, K.-T., A Low Energy Gap Organic Dye for High-Performance Small Molecule Organic Solar Cells. *J. Am. Chem. Soc.* **2011,** *133*, 15822-15825.

(2) Jung, I.; Yu, J.; Jeong, E.; Kim, J.; Kwon, S.; Kong, H.; Lee, K.; Woo, H.; Shim, H., Synthesis and Photovoltaic Properties of Cyclopentadithiophene-Based Low-Bandgap Copolymers That Contain Electron-Withdrawing Thiazole Derivatives. *Chem. Eur. J.* **2010**, *16*, 3743-3752.

(3) Holliday, S.; Ashraf, R. S.; Nielsen, C. B.; Kirkus, M.; Rohr, J. A.; Tan, C. H.; Collado-Fregoso, E.; Knall, A. C.; Durrant, J. R.; Nelson, J.; McCulloch, I., A Rhodanine Flanked Nonfullerene Acceptor for Solution-Processed Organic Photovoltaics. *J. Am. Chem. Soc.* **2015**, *137*, 898-904.

(4) Frisch, M. J.; Trucks, G. W.; Schlegel, H. B.; Scuseria, G. E.; Robb, M. A.; Cheeseman, J. R.; Scalmani, G.; Barone, V.; Mennucci, B.; Petersson, G. A.; Nakatsuji, H.; Caricato, M.; Li, X.;Hratchian, H. P.; Izmaylov, A. F.; Bloino, J.; Zheng, G.; Sonnenberg, J. L.; Hada, M.; Ehara, M.;Toyota, K.; Fukuda, R.; Hasegawa, J.; Ishida, M.; Nakajima, T.; Honda, Y.; Kitao, O.; Nakai, H.;Vreven, T.; Montgomery Jr., J. A.; Peralta, J. E.; Ogliaro, F.; Bearpark, M. J.; Heyd, J.; Brothers, E. N.; Kudin, K. N.; Staroverov, V. N.; Kobayashi, R.; Normand, J.; Raghavachari, K.; Rendell, A. P.; Burant, J. C.; Iyengar, S. S.; Tomasi, J.; Cossi, M.; Rega, N.; Millam, N. J.; Klene, M.; Knox, J. E.; Cross, J. B.; Bakken, V.; Adamo, C.; Jaramillo, J.; Gomperts, R.; Stratmann, R. E.; Yazyev, O.; Austin, A. J.; Cammi, R.; Pomelli, C.; Ochterski, J. W.; Martin, R. L.; Morokuma, K.; Zakrzewski, V. G.; Voth, G. A.; Salvador, P.; Dannenberg, J. J.; Dapprich, S.; Daniels, A. D.; Farkas, Ö.; Foresman, J. B.; Ortiz, J. V.; Cioslowski, J.; Fox, D. J. *Gaussian 09, Revision C.01*, Gaussian, Inc.: Wallingford, CT, USA, **2009**.

(5) Risko, C.; McGehee, M. D.; Bredas, J.-L., A Quantum-chemical Perspective into Low Optical- gap Polymers for Highly-Efficient Organic Solar Cells. *Chem. Sci.* **2011**, *2*, 1200-1218.

(6) Pandey, L.; Risko, C.; Norton, J. E.; Brédas, J.-L., Donor–Acceptor Copolymers of Relevance for Organic Photovoltaics: A Theoretical Investigation of the Impact of Chemical Structure Modifications on the Electronic and Optical Properties. *Macromolecules* **2012**, *45*, 6405-6414.

(7) Douglas, J. D.; Chen, M. S.; Niskala, J. R.; Lee, O. P.; Yiu, A. T.; Young, E. P.; Frechet, J. M., Solution-Processed, Molecular Photovoltaics That Exploit Hole Transfer from Non-Fullerene, N-Type Materials. *Adv. Mater.* **2014,** *26*, 4313-4319.

(8) Cardona, C. M.; Li, W.; Kaifer, A. E.; Stockdale, D.; Bazan, G. C., Electrochemical Considerations for Determining Absolute Frontier Orbital Energy Levels of Conjugated Polymers for Solar Cell Applications. *Adv. Mater.* **2011,** *23*, 2367-2371.

(9) Jagadamma, L. K.; Abdelsamie, M.; El Labban, A.; Aresu, E.; Ngongang Ndjawa, G. O.; Anjum, D. H.; Cha, D.; Beaujuge, P. M.; Amassian, A., Efficient Inverted Bulk-Heterojunction Solar Cells from Low-Temperature Processing of Amorphous Zno Buffer Layers. *J. Mater. Chem. A* **2014,** *2*, 13321-13331.

(10) Pettersson, L.; Roman, L.; Inganäs, O., Modeling Photocurrent Action Spectra of Photovoltaic Devices based on Organic Thin Films. *J. Appl. Phys.* **1999**, *86*, 487-496.

(11) Johs, B.; Hale, J., Dielectric Function Representation by B-splines. *Phys. Stat. Sol.* **2008**, *205*, 715-719.

(12) Liu, S.; Zhang, K.; Lu, J.; Zhang, J.; Yip, H.-L.; Huang, F.; Cao, Y., High-efficiency Polymer Solar Cells via the Incorporation of an Amino-Functionalized Conjugated Metallopolymer as a Cathode Interlayer. *J. Am. Chem. Soc.* **2013**, *135*, 15326-15329.
(13) Murgatroyd, P. N., Theory of space-charge-limited current enhanced by Frenkel effect. *J. Phys. D: Appl. Phys.* **1970**, 3.2, 151.